Simulation Study on the Static Characteristics of 'Five-tier Outer Eave Column-head Dougong Bracket' from the Main Hall of Nanchan Temple in Tang Dynasty

Chang Chen,[a] Yuanhe Li,[a] Dongnan Han,[a,*] Hongfa Kang,[a] and Yongzheng Li [b]

The static structural behavior was investigated for the 'Five-tier Outer Eave Column-head Dougong bracket' from the Main Hall of Nanchan Temple (Tang Dynasty of ancient China) using finite element analysis (FEA). A refined ANSYS model was developed with an orthotropic constitutive framework based on mechanical properties of *Pinus sylvestris* (tested per GB/T standards), incorporating the Hill yield criterion to define wood plasticity. Vertical monotonic static loading (Z-axis) and horizontal low-cycle reciprocating loading (Y- and X-axes) were simulated to evaluate strength, deformation, and energy dissipation. Results revealed a vertical ultimate bearing capacity of 338 kN (Z-axis) with stress concentrations at the column-head/base-block interface (21.8 MPa). Horizontal loading demonstrated symmetric hysteresis loops, yielding peak thrusts of 1,417 kN (Y-axis) and 747 kN (X-axis), accompanied by ductility coefficients of 2.53 and equivalent viscous damping coefficients of 0.096 (Y-axis) and 0.073 (X-axis). The vertical response followed a tri-linear stiffness degradation model, while horizontal behavior aligned with multi-linear restoring force models. These findings validate FEA as a cost-effective method for characterizing Dougong mechanics, providing critical insights for heritage timber structure conservation.

DOI: 10.15376/biores.20.3.6082-6099

Keywords: Dougong bracket; Wood component; Static characteristics; Finite element simulation; Pinus sylvestris

*Contact information: a: School of Architecture and Art Design, Inner Mongolia University of Science & Technology, Baotou 014010, P.R. China; b: Inner Mongolia Zhongyu Aerospace Engineering Planning and Design Co., Ltd., Baotou 014010, P.R. China; *Corresponding author: 872447850@qq.com*
Chang Chen and Yuanhe Li contributed equally to this work.

INTRODUCTION

The Main Hall of Nanchan Temple (Fig. 1) is located in Wutai County, Shanxi Province, China. Constructed in 782 CE during the Tang Dynasty's Jianzhong era, the Main Hall of Nanchan Temple stands as one of China's earliest surviving timber-frame structures, exemplifying the dynasty's architectural ethos through its majestic simplicity that achieves an unparalleled synthesis of mechanical efficiency and aesthetic refinement. The Dougong, a unique structural component in ancient Chinese wooden architecture, serves as a transitional element between columns and roof systems by extending eaves projection, reducing beam spans, and transferring roof loads to vertical supports through its bracket cluster configuration (Fang *et al*. 2001; D'Ayala and Tsai 2008; Cao *et al*. 2021). 'Tier' is a concept used to describe the structural characteristics of the overlapping layers of Dougong in ancient Chinese wooden architecture system, in which the number of tiers indicates the number of jumps. The structural configuration of Dougong brackets is defined

by the 'jumps' system, where each horizontal projection initiating from the base block (Fig. 2b) – whether formed by arch arms (Fig. 2c) or ang cantilevers (Fig. 2d) – constitutes a discrete jump, with historical specimens demonstrating up to five sequential jumps to maintain structural integrity under traditional architectural proportioning principles. According to the naming method of Dougong of ancient Chinese wooden architecture system, one jump is called four-tier, two jumps are called five-tier, three jumps are called six-tier, four jumps are called seven-tier, and five jumps are called eight-tier. Therefore, the number of jumps plus three is Dougong's tier number. The authentic outer eave column-head dougong bracket in the Main Hall of Nanchan Temple (Fig. 3) is a five-tier Dougong, that is, two jumps from the base block.

Fig. 1. The Main Hall of Nanchan temple

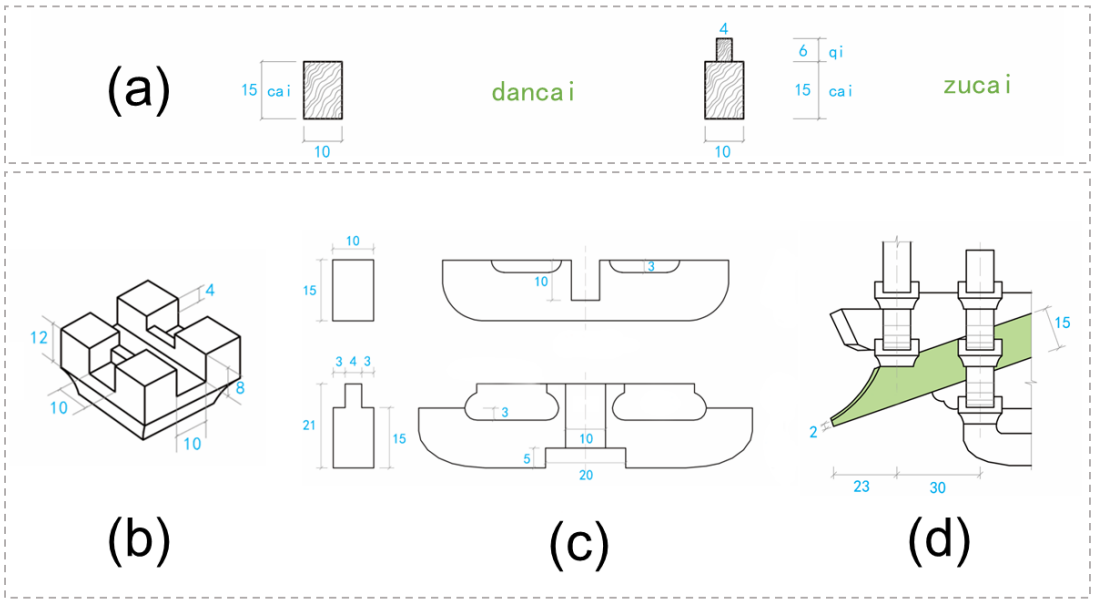

Fig. 2. The cai-fen system (a), base block (b), arch arm (c), and ang cantilever (d) of Dougong brackets

The *cai-fen* system (cai and fen) constitutes the modular basis for timber construction in ancient China. In that system, the term *fen* represents a proportional unit rather than a specific geometric dimension. As defined in the Song dynasty architectural treatise *Yingzao Fashi*, the *cai* refers to a rectangular section with a height of 15 *fen* and a width of 10 *fen* (Fig. 2a). Mortise blocks, termed *qi*, with a height of 6 *fen*, were inserted between consecutive *cai* sections to facilitate joinery. A combined height of one *cai* plus one *qi* (21 *fen*) is designated as a *zucai* (full-height timber) (Fig. 2a), while the height of a single *cai* (15 fen) is termed a *dancai* (single-height timber) (Fig. 2a). Overall building dimensions, the sizing of structural members, and the methods for determining roof curvature (*juzhe*) were standardized using the *cai* as the fundamental unit of measure. The opening on the base block (Fig. 2b) of dougong bracket along the facade direction is called the *doukou* (mortise), sharing the same 10 *fen* width as the *cai*. Consequently, ancient Chinese timber-frame architecture also employed the *doukou* as a primary module. The Song system classified *cai* into eight grades (*deng*), allocated for structures of different scales (Xue *et al*. 2016; Wu *et al*. 2018; Sha *et al*. 2021). The research object of this paper comes from the provisions of the *Yingzao Fashi* of the Song Dynasty. The *Yingzao Fashi* clearly stipulates the structural form of the first to eight-class timber and the detailed dimensions of each component in the Dougong bracket. The *fen* corresponding to grades one through eight in *Yingzao Fashi*, when converted to the metric system, are precisely 18.53, 17.00, 15.47, 14.80, 13.60, 12.33, 10.80, and 9.27 mm. The object of this study is second-class timber, of which the *fen* is equal to 17 mm. A perspective view and an explosion diagram of the outer eave column-head dougong of the Main Hall of Nanchan Temple test model of the second-class is shown in Fig. 4. In the Dougong bracket, there are a total of 40 units including 24 main parts and 16 wood pins, which are divided into two types.

Fig. 3. The authentic outer eave column-head dougong bracket in the Main Hall of Nanchan Temple

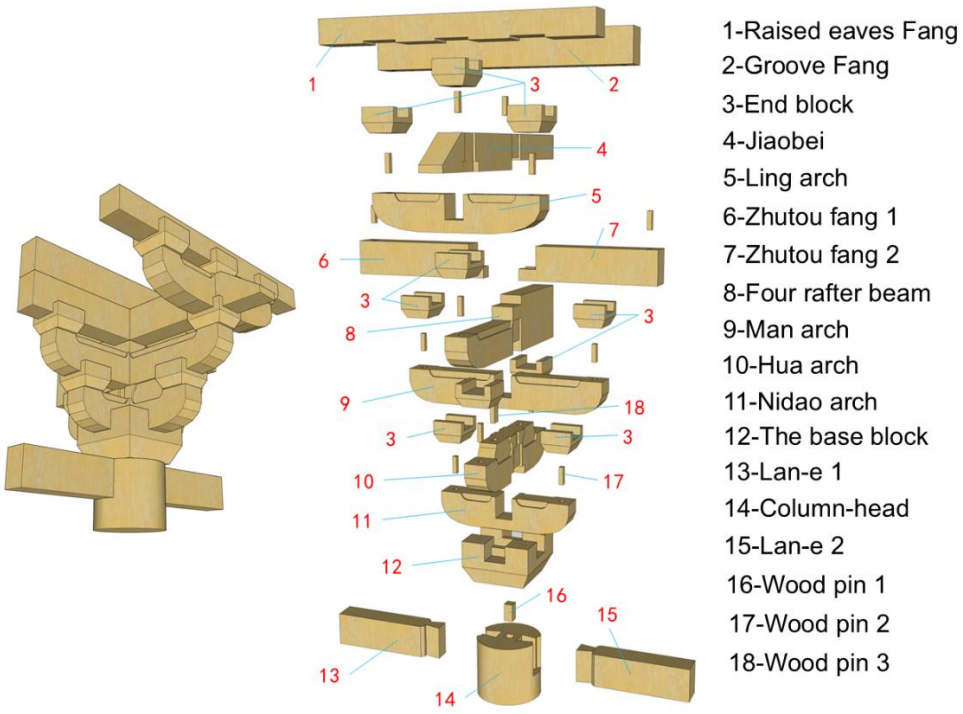

Fig. 4. The perspective view (left) and explosion diagram (right) of the outer eave column-head dougong of the Main Hall of Nanchan Temple test model

In traditional timber structure testing, the production of full-scale models of Dougong brackets incurs substantial costs (Chen *et al*. 2018; Meng *et al*. 2019). Conventional experimental methods, which rely on instrumented measuring points, are constrained by uncontrollable errors and inherent limitations in structural testing accuracy. However, finite element analysis (FEA)-based simulation technology has proven effective in analyzing the static characteristics of Dougong brackets, supported by decades of development and extensive structural testing (Suzuki and Maeno 2006; Bedon *et al*. 2015; Wu *et al*. 2020). Notably, this approach circumvents the high costs associated with specimen fabrication while enabling targeted investigations, particularly in evaluating the static behavior of full-scale models (Sciomenta *et al*. 2018).

In this study, the static structural behavior of a refined Five-tier Outer Eave Column-head Dougong bracket was systematically investigated using finite element software ANSYS. Key mechanical indices—including strength, deformation, and energy dissipation—were simulated to comprehensively characterize the bracket's performance under static loading conditions. This methodology provides a cost-efficient and precise alternative to traditional experimental approaches, advancing the understanding of Dougong mechanics in heritage timber structures.

EXPERIMENTAL

Material Property Test of *P. sylvestris*

The simulation utilized *P. sylvestris* as the material, with its mechanical properties evaluated at 12% moisture content through standardized tests. Following GB/T 1933 (2009), the air-dry density was determined as 0.493 g/cm³. Elastic modulus, Poisson's

ratio, and shear modulus were measured using the resistance strain method in compliance with GB/T 15777 (2017), GB/T 1943 (2009), and LY/T 3297 (2022), with results detailed in Table 1. Strength parameters included a compressive strength of 35.2 MPa parallel to grain (GB/T 1935, 2009), 5.14 MPa perpendicular to grain (GB/T 1939, 2009), and a bending strength of 52.9 MPa (GB/T 1936.1, 2009). In the Dougong bracket system, transverse grain compression predominates across components. To mitigate structural defects such as knots and decay, strategic grain realignment was implemented during material preparation, optimizing mechanical performance while preserving structural integrity through adaptive grain orientation.

Table 1. The Elastic Modulus, Poisson's Ratio, and Shear Modulus of *P. sylvestris*

	E_L	E_R	E_T	V_{LR}	V_{LT}	V_{RT}	G_{LR}	G_{LT}	G_{RT}
P. sylvestris	8023	1103	843	0.422	0.513	0.687	652	345	231

* E_L is the linear elastic modulus, MPa; E_R is the horizontal radial elastic modulus, MPa; and E_T is the horizontal tangential elastic modulus, MPa. V_{LR} is the Poisson's ratio of longitudinal extension stress, V_{LT} is the Poisson's ratio of transverse radial extension stress, and V_{RT} is the Poisson's ratio of transverse tangential extension stress. G_{LR} is the longitudinal-radial shear modulus, MPa; G_{LT} is the longitudinal-chordal shear modulus, MPa; and G_{RT} is the horizontal shear modulus, MPa.

Material Parameter Configuration and Orthotropic Constitutive Modeling in Simulation

The Dougong bracket simulation was developed using FEA within ANSYS Workbench 2021 R1 (ANSYS, Inc., San Diego, USA). Material parameters were rigorously implemented based on experimental test results, with plasticity and elasticity definitions derived from the measured stress-strain curves and the Hill yield criterion. Figure 5a illustrates the fitted stress-strain relationships for *P. sylvestris* under longitudinal, radial transverse, and tangential transverse loading orientations.

An orthotropic constitutive model (Fig. 5b) was adopted to represent the wood's three-dimensional mechanical behavior, defined by nine independent elastic coefficients within the elastic matrix. These coefficients, corresponding to the material's three orthogonal symmetry planes (longitudinal, radial, and tangential), were systematically input into ANSYS to establish the computational framework. Three key aspects were implemented: Elasticity: Direction-dependent Young's moduli (EL, ER, ET), shear moduli (GLR, GLT, GRT), and Poisson's ratios (ν-LR, ν-LT, ν-RT) derived from experimental data. Plasticity: Hill's anisotropic yield criterion calibrated using multiaxial strength ratios (σ-parallel/σ-perpendicular = 6.85). Failure Criteria: Stress thresholds aligned with measured compressive (35.2 MPa parallel, 5.14 MPa perpendicular) and flexural (52.9 MPa) strengths.

This modeling approach explicitly accounts for the orthotropic nature of wood, enabling accurate replication of its direction-dependent stiffness, strength asymmetry, and nonlinear deformation characteristics under complex loading scenarios. The constitutive framework was validated through iterative comparison with experimental stress-strain responses, ensuring fidelity in simulating the Dougong system's mechanical performance.

(a)

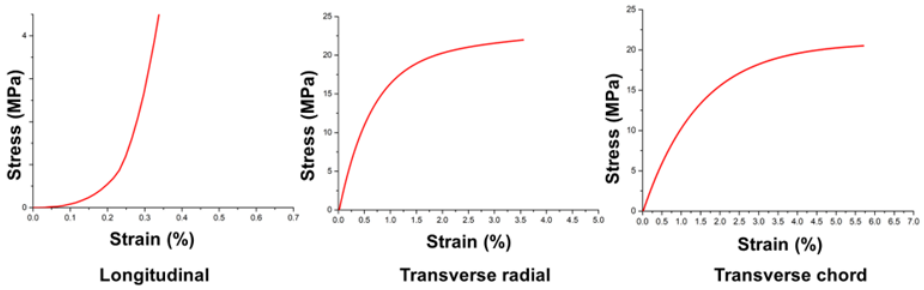

(b)

$$\begin{Bmatrix}\sigma_{11}\\ \sigma_{22}\\ \sigma_{33}\\ \sigma_{12}\\ \sigma_{13}\\ \sigma_{23}\end{Bmatrix} = \begin{bmatrix} D_{1111} & D_{1122} & D_{1133} & 0 & 0 & 0 \\ & D_{2222} & D_{2233} & 0 & 0 & 0 \\ & & D_{3333} & 0 & 0 & 0 \\ & & & D_{1212} & 0 & 0 \\ & sym & & & D_{1313} & 0 \\ & & & & & D_{2323} \end{bmatrix} \begin{Bmatrix}\varepsilon_{11}\\ \varepsilon_{22}\\ \varepsilon_{33}\\ \gamma_{12}\\ \gamma_{13}\\ \gamma_{23}\end{Bmatrix} = [D^{el}] \begin{Bmatrix}\varepsilon_{11}\\ \varepsilon_{22}\\ \varepsilon_{33}\\ \gamma_{12}\\ \gamma_{13}\\ \gamma_{23}\end{Bmatrix}$$

$$\begin{aligned} D_{1111} &= E_1(1-\nu_{23}\nu_{32})r, \\ D_{2222} &= E_2(1-\nu_{13}\nu_{31})r, \\ D_{3333} &= E_3(1-\nu_{12}\nu_{21})r, \\ D_{1122} &= E_1(\nu_{21}+\nu_{31}\nu_{23})r = E_2(\nu_{12}+\nu_{32}\nu_{13})r, \\ D_{1133} &= E_1(\nu_{31}+\nu_{21}\nu_{32})r = E_3(\nu_{13}+\nu_{12}\nu_{23})r, \\ D_{2233} &= E_2(\nu_{32}+\nu_{12}\nu_{31})r = E_3(\nu_{23}+\nu_{21}\nu_{13})r, \end{aligned} \qquad \begin{aligned} D_{1212} &= G_{12}, \\ D_{1313} &= G_{13}, \\ D_{2323} &= G_{23}, \\ r &= \frac{1}{1-\nu_{12}\nu_{21}-\nu_{23}\nu_{32}-\nu_{31}\nu_{13}-2\nu_{21}\nu_{32}\nu_{13}}. \end{aligned}$$

Fig. 5. Stress/strain curves of the longitudinal, transverse radial, and transverse chord of *P. sylvestris* (a) and wood orthotropic constitutive model (b)

Loading Protocol

The vertical loading protocol was derived from permanent roof load calculations based on historical architectural specifications and structural analysis (Niu 2017), focusing on static characteristics of the Dougong bracket itself; dynamic or transient loads (*e.g.*, occupants, snow) were excluded to isolate fundamental structural behavior under idealized static conditions. Based on the coordinate axis orientation defined for the test model (Fig. 6b), vertical monotonic static loading (Chen *et al*. 2014) was applied along the Z-axis, while horizontal low-cycle reciprocating loading (Fujita *et al*. 2001; Meng *et al*. 2018) was imposed in both the Y-axis and X-axis directions.

Vertical monotonic static loading tests were conducted following the experimental protocol established by Niu (2017) for simulating permanent roof load transfer mechanisms in traditional Chinese Dougong system. The initial vertical load was set at 60 kN, representing the calculated permanent roof load value derived from architectural specifications and structural analysis. A force-displacement hybrid control methodology was implemented in two sequential phases. During the initial phase, force-controlled loading was applied at a constant rate of 5 kN/min until specimen yielding occurred, as determined by visible deformation or significant nonlinearity in the load-displacement curve. Subsequently, the test transitioned to displacement-controlled loading at 2 mm/min to investigate post-yield behavior. The termination criteria for the second phase included either specimen collapse (characterized by load capacity reduction to 80% of peak resistance) or severe structural damage preventing further load application. This two-stage approach ensured comprehensive characterization of both elastic and plastic deformation characteristics while maintaining experimental control throughout the failure progression.

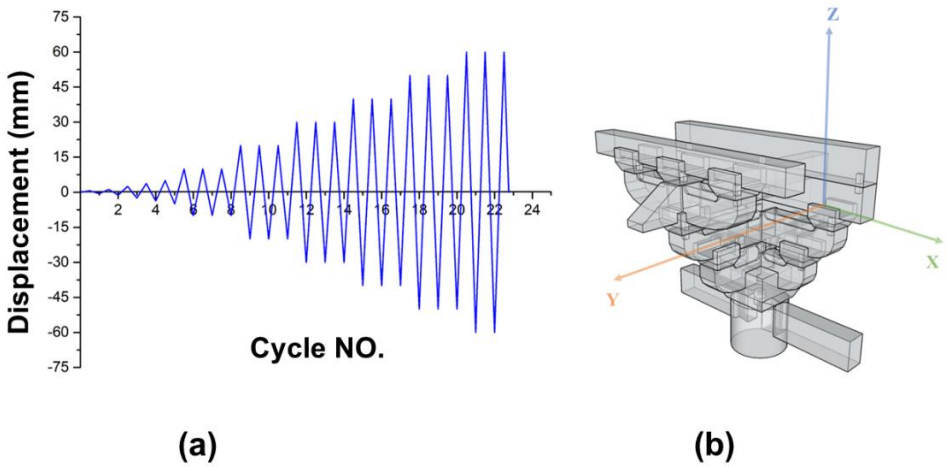

Fig. 6. The direction definition of the test model in the coordinate axis and its loading protocol

A quasi-static test under horizontal low-cycle reciprocating loading was conducted using displacement-controlled protocols (Yao and Li 2023). The loading regime comprised two phases: Initial phase - Five monotonic reciprocating cycles with progressively increasing amplitudes (0.0125Δ, 0.025Δ, 0.05Δ, 0.075Δ, and 0.1Δ, where Δ = 50 mm); Secondary phase - Three reciprocating cycles per amplitude level starting from 0.2Δ, with incremental amplitude increases of 0.2Δ per step (Cao *et al*. 2021). The loading protocol is illustrated in Fig. 6a. Solver configurations, connection relationships, and boundary conditions in the numerical simulations were rigorously aligned with experimental setups along the Z-, Y-, and X-axes (Fig. 6b).

Grid System

The grid system was constructed using second-order elements, employing a hybrid hexahedral-tetrahedral meshing strategy. Geometrically regular regions were discretized with hexahedral elements, while tetrahedral elements were applied to complex geometries. The final assembled grid system of the Dougong bracket is presented in Fig. 7.

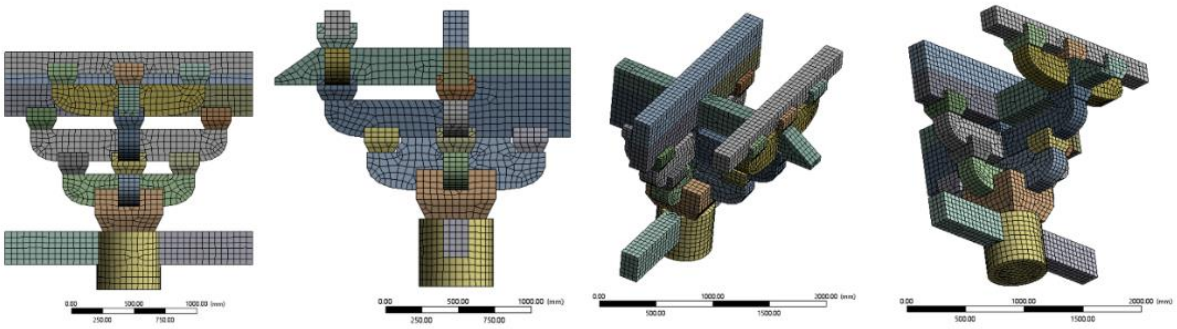

Fig. 7. Division of Dougong bracket's grid system in simulation

RESULTS AND DISCUSSION

Vertical Monotonic Static Loading (Z-axis)

The load-displacement curve obtained by the vertical monotonic loading simulation in the Z-axis direction is shown in Fig. 8. The bearing capacity of Dou-Gong bracket model obtained by the simulation does not converge after 338 kN. The Von Mises stress distribution (Fig. 9A) in the Tang Dynasty Dougong under Z-axis loading exhibited predominant concentration in upper structural elements along the loading axis. Peak stress magnitude of 21.75 MPa was localized at the base block/column-head interface, corresponding to the central mortise-tenon joint.

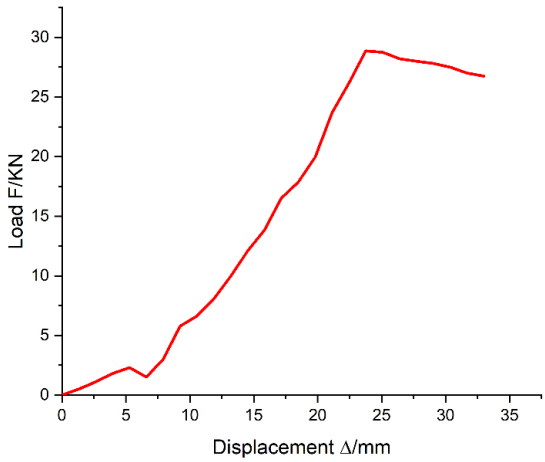

Fig. 8. The load-displacement curve in Z-axis

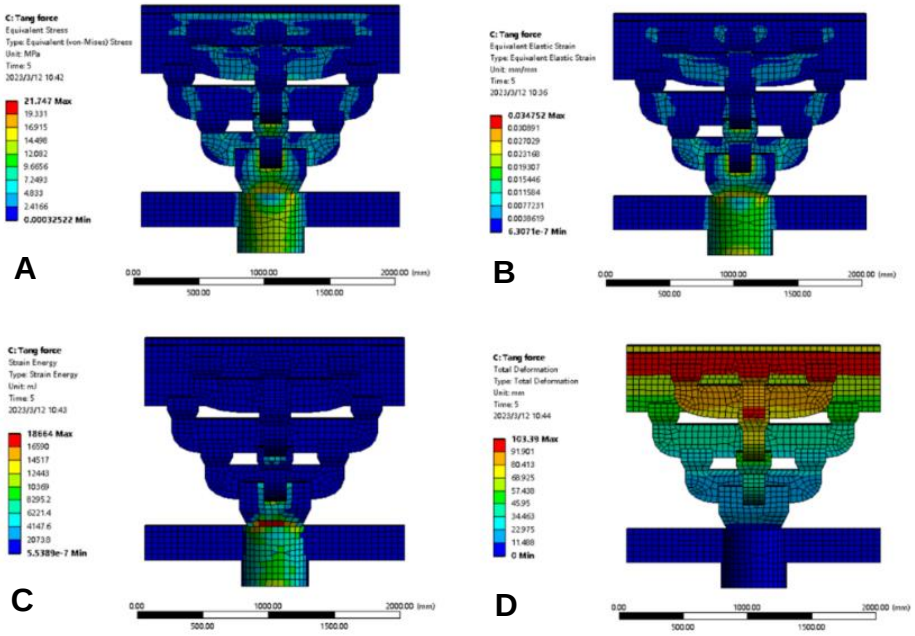

Fig. 9. The Von Mises stress distribution, the equivalent elastic strain distribution, the strain energy density distribution and displacement analysis in Z-axis

Congruent distribution patterns were observed in the equivalent elastic strain distribution (Fig. 9B), with maximum strain values of 0.0340 occurring at this critical structural interface. Strain energy density distribution (Fig. 9C) demonstrated spatial consistency with stress concentrations, accumulating 18,664 MJ at the base block/column-head complex.

This energy focalization confirms the Dougong's effective load transfer mechanism from upper elements to supporting columns. Displacement analysis (Fig. 9D) revealed a progressive deformation gradient decreasing from 103.4 mm at the Raised Eaves Fang apex to minimal values at the foundation, consistent with the hierarchical deformation characteristics of traditional timber structures under vertical loading.

Horizontal Low-cycle Reciprocating Loading (Y-axis and X-axis)

The simulation results of the horizontal low-cycle reciprocating load tests along the Y- and X-axis directions are presented in Fig. 10, demonstrating the load-displacement hysteresis characteristics of the Dougong bracket. The experimental model exhibits a peak lateral load capacity of 1,417 kN in the Y-axis direction and 747 kN in the X-axis direction. Both axial hysteresis curves display symmetrical full spindle-shaped patterns, indicating robust plastic deformation capacity and substantial energy dissipation efficiency under cyclic loading. This hysteretic behavior confirms the structure's exceptional seismic resilience through two distinct mechanisms: the pronounced ductility evidenced by stable strength retention during cyclic degradation phases, and the elevated equivalent viscous damping coefficients that effectively mitigate sudden brittle failures. Notably, the spindle-shaped hysteresis characteristics suggest optimized stress redistribution mechanisms in wooden components subjected to combined bending-shear-compression actions, where progressive fiber realignment and interfacial friction energy dissipation prevent abrupt shear plane development. These findings align with contemporary timber mechanics research emphasizing the importance of ductile failure modes in traditional wooden structures.

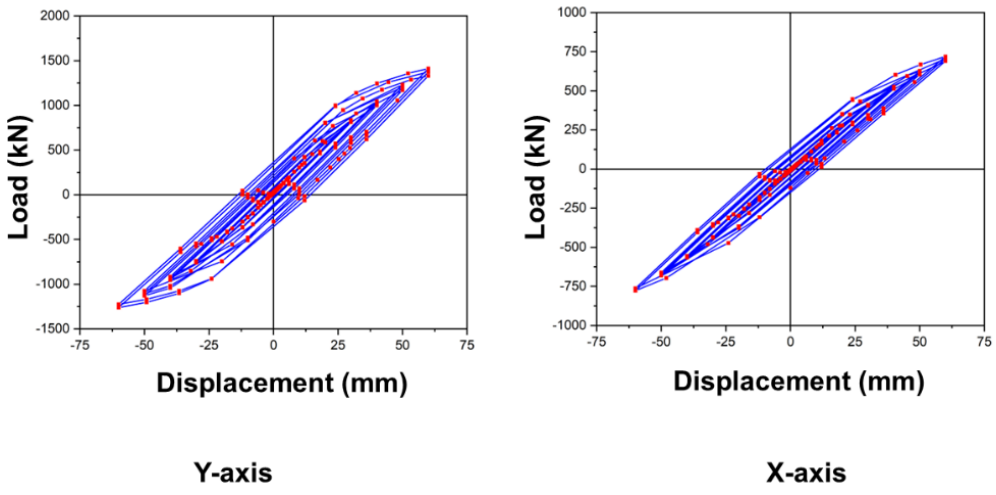

Fig. 10. The load-displacement hysteretic curves in Y-axis and X-axis

According to hysteretic curve, the load-displacement skeleton curve can be obtained (Fig. 11), and the stiffness degradation curve of the specimen is obtained by extracting the stiffness of each section of the skeleton curve (Fig. 12).

The Von Mises stress distribution (Fig. 13A) exhibited pronounced stress concentrations predominantly localized at the interface between the rear terminus of Four-rafter-beam and the Hua arm-column head connection. The peak stress magnitude reached 37.25 MPa, specifically observed at the mortise-tenon joint of the four-rafter rear end and the loose bucket component. A congruent spatial pattern was identified in the equivalent elastic strain distribution (Fig. 13B), with maximum strain values of 0.0446 concentrated at this critical structural interface.

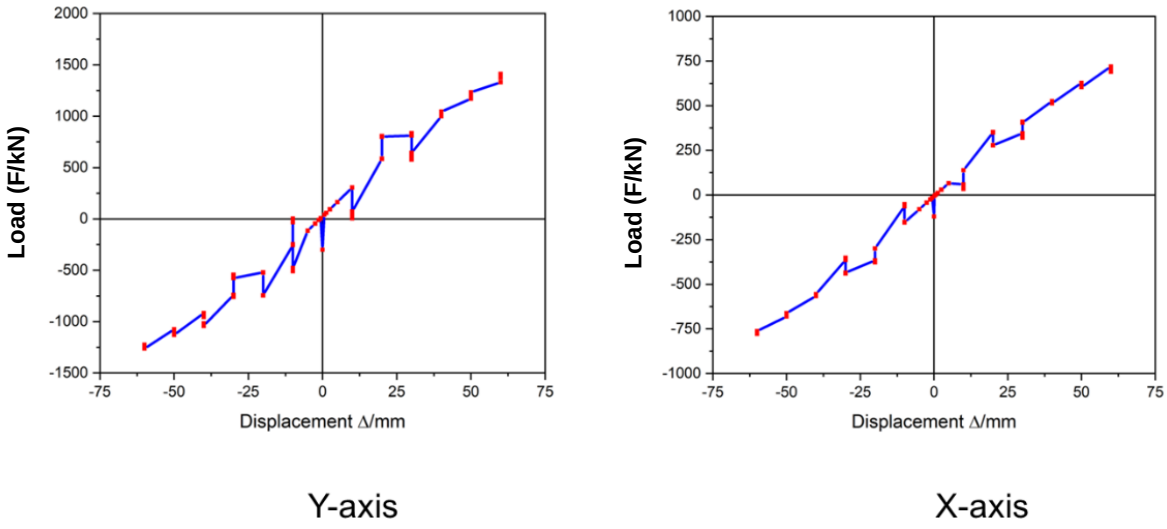

Fig. 11. The load-displacement skeleton curves in Y-axis and X-axis

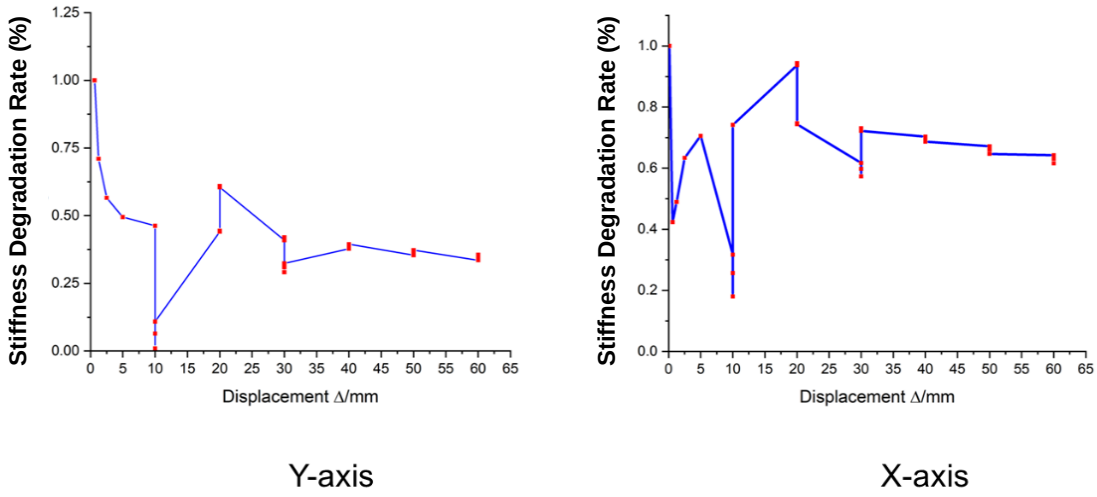

Fig. 12. The stiffness degradation curves in Y-axis and X-axis

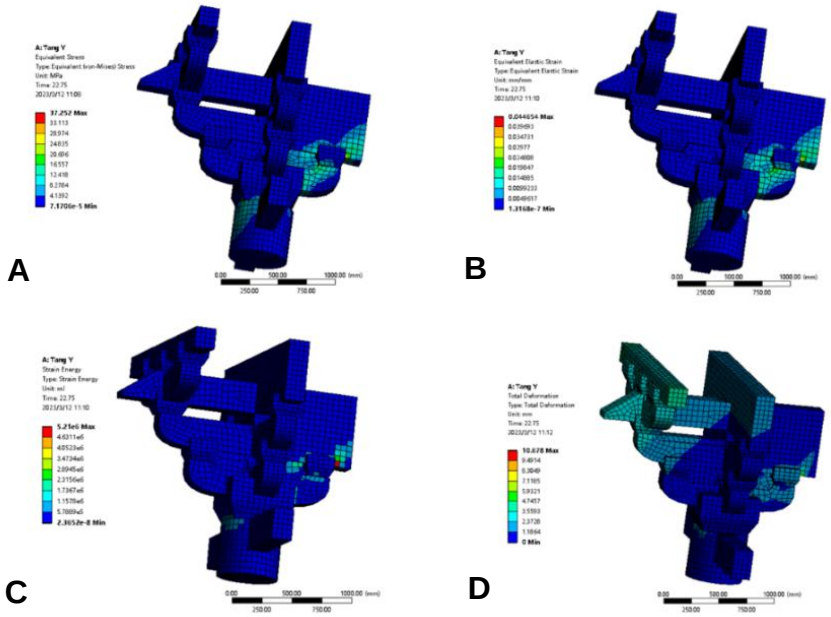

Fig. 13. The Von Mises stress distribution, the equivalent elastic strain distribution, the strain energy density distribution, and displacement analysis in Y-axis

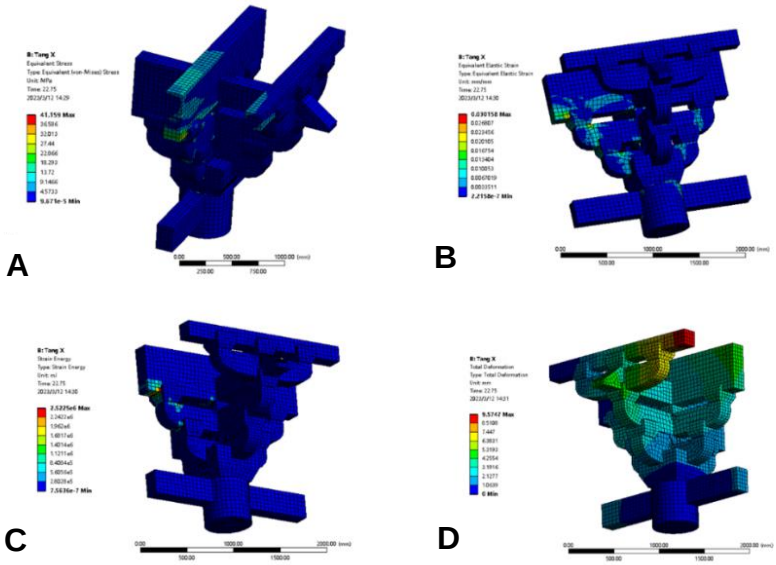

Fig. 14. The Von Mises stress distribution, the equivalent elastic strain distribution, the strain energy density distribution, and displacement analysis in X-axis

Strain energy density distribution (Fig. 13C) demonstrated topological consistency with the stress field, confirming effective energy transfer through the arch-rafters-bucket structural system to the supporting columns. The maximum accumulated strain energy of 5.21×10^6 MJ was recorded at the four-rafter/bucket mortise joint, establishing this region as the primary energy dissipation zone. Displacement analysis (Fig. 13D) revealed a hierarchical deformation pattern: maximum displacement of 10.678 mm occurred at the four-rafter/bucket tenon connection, with secondary deformation gradients distributed across the Raised eaves Fang, Ling arch, and base block-column head interfaces.

The Von Mises stress distribution (Fig. 14A) under quasi-static X-axis loading

revealed critical stress concentration at the mortise-tenon interface between the left column-head beam and bucket component, with peak stress magnitude reaching 41.16 MPa. This stress localization correlates with the equivalent elastic strain distribution (Fig. 14B), which exhibited maximum values of 0.0301 at the Man arch/End block joint, confirming the spatial congruence between stress and strain fields. The strain energy density distribution (Fig. 14C) mirrored the stress concentration pattern, accumulating 2.52×10^6 MJ at the Zhutou fang/End block interface. This energy focalization suggests the mortise-tenon joint acts as the primary energy dissipation zone during cyclic loading. Displacement analysis (Fig. 14D) demonstrated maximum deformation of 9.574 mm at Raised eaves Fang's right terminus, while structural deformation gradients decreased progressively toward the foundation, consistent with traditional timber structure deformation mechanisms under lateral loading.

Notably, the combined stress-strain-energy triad indicates potential failure initiation at the column-head/ End block interface, where both mechanical stress (41.16 MPa) and strain energy density (2.52×10^6 MJ) exceed critical thresholds observed in similar timber joints. This failure mechanism aligns with reported damage patterns in historical timber structures subjected to cyclic lateral loads.

Mechanical Model of Static Structural Behavior (Z-axis, Y-axis, and X-axis)

The five-tiered outer eave column-head Dougong specimen exhibited a tri-linear elastic stiffness degradation model under Z-axis monotonic loading (Fig. 15), characterized by three distinct mechanical phases. In Phase OA (0–ΔA), initial gap closure between components induced contact nonlinearity, resulting in low structural stiffness (K_{OA} = 2.66 kN/mm, calculated *via* Eq. 1). Phase AB (ΔA–ΔB) demonstrated linear elastic behavior with stabilized stiffness (K_{AB} = 4.48 kN/mm, derived from Eq. 2), marked by fully established component interactions. Progressive stiffness degradation (K_{BC} = 3.07 kN/mm, per Eq. 3) dominated Phase BC (ΔB–ΔC), attributed to mortise-tenon joint yielding and structural damage accumulation.

$$k_{OA} = \frac{P_x}{\Delta_x} \quad (1)$$

$$k_{AB} = \frac{P_y - P_x}{\Delta_y - \Delta_x} \quad (2)$$

$$k_{BC} = \frac{P_b - P_y}{\Delta_b - \Delta_y} \quad (3)$$

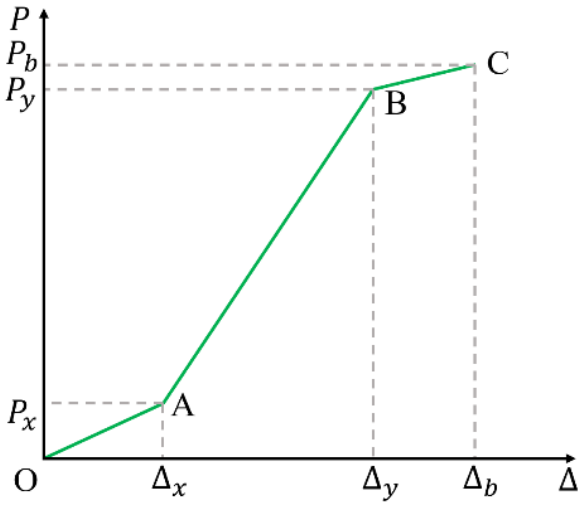

Fig. 15. The tri-linear elastic stiffness degradation model under Z-axis monotonic loading

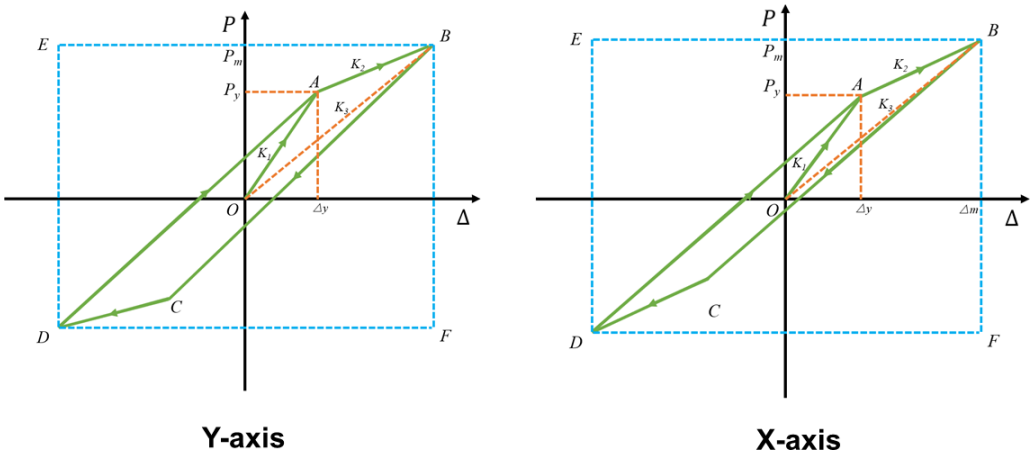

Fig. 16. The restoring force model of the static structural behavior in Y-axis and X-axis

According to the hysteresis curve and skeleton curve, the restoring force model (Fig. 16) of the static structural behavior of the five-tiered outer eave column-head Dougong test model on the Y axis and X axis is established.

On the Y axis, OA is the elastic stage, the displacement of the test model is proportional to the load, and the stiffness K_{Y1} is 40.13 kN/mm; AB is the yield stage, from point A to point B, the stiffness K_{Y2} of the test model in the plastic stage is 8.89 kN/mm; K_{Y3} is the ratio of the maximum bearing capacity to the maximum displacement of the restoring force model, which is called the effective stiffness of Dougong bracket. The effective stiffness K_{Y3} of the test model is 21.51 kN/mm. The static structural behavior of Dougong bracket test model on the X-axis is similar to that of the Y-axis. The stiffness K_{X1} of OA in the elastic stage, the stiffness K_{X2} of AB in the yield stage, and the effective stiffness K_{X3} are 20.72, 6.63, and 12.09 kN mm, respectively.

If the Dougong bracket component is regarded as the shock absorber between the roof and the column of the ancient Chinese timber structure, the nonlinear coefficient NL can be introduced to quantitatively evaluate the damping effect. NL is equal to the ratio of the envelope area of the restoring force model to the rectangular area S_{BDEF} in Fig. 16. NL

can characterize the energy dissipation capacity of Dougong bracket component. The nonlinear coefficient NL of five-tiered outer eave column-head Dougong test model in the Y-axis direction is 0.172, and the nonlinear coefficient NL in the X-axis direction is 0.115.

The ratio of ultimate displacement and yield displacement of Dougong bracket is the ductility of the component, and the greater ductility reflects that the component has better deformation ability. The ductility of five-tiered outer eave column-head Dougong test model in the Y-axis direction is 2.53, and the ductility in the X-axis direction is 2.53 according to the simulation results.

The larger the equivalent viscous damping coefficient (h_e) is, the stronger the energy dissipation capacity of Dougong bracket component is. The equivalent viscous damping coefficient is calculated according to Fig. 17 and Eq. 4. The equivalent viscous damping coefficient of five-tiered outer eave column-head Dougong Bracket test model in the Y-axis direction is 0.096, and the equivalent viscous damping coefficient in the X-axis direction is 0.073.

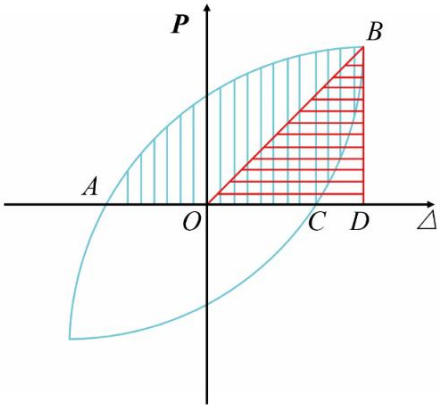

Fig. 17. Calculation of equivalent viscous damping coefficient

$$h_e = \frac{1}{2\pi} \cdot \frac{S_{ABC}}{S_{OBD}} \quad (4)$$

The static structural performance and stress-deformation characteristics of the Five-tier Outer Eave Column-head Dougong Bracket test model from Nanchan Temple's Main Hall were evaluated through three-dimensional analysis (X, Y, Z axes). Under vertical monotonic static loading along the Z-axis, the structural behavior follows a variable-stiffness linear elastic mechanics model, demonstrating three distinct phases: Phase I involves compaction of inter-component gaps and nodal connections. Phase II exhibits linear load-displacement proportionality with stable stiffness. Phase III manifests structural yielding leading to ultimate failure. For horizontal low-cycle reciprocated loading in Y and Z axes, the behavior aligns with a multi-linear restoring force model, progressing through elastic, yielding, and failure stages. Loading progression reveals gradual stiffness degradation in the Dougong bracket system. Hysteresis loops demonstrate pinching characteristics near the coordinate origin, indicating slippage phenomena. Post-critical horizontal loading induces severe plastic deformation accompanied by abrupt displacement amplification. Key mechanical parameters quantifying static performance were obtained through triaxial evaluation of strength characteristics, deformation capacity, and energy dissipation efficiency, as systematically presented in Table 2. The experimental results reveal that structural damage initiates at critical nodes under excessive loading, with subsequent force redistribution accelerating system collapse.

Table 2. Characteristic Values of the Six Specimen Configurations

Name	Qing-style 'One Bucket Three Liters' Column-cap Dou-Gong Bracket						
Pathway	Numerical Simulation						
Intensity		Deformation				Energy Dissipation	
F_{Z1}	F_{Z2}	K_{Z1}	K_{Z2}	K_{Z3}		NL(Y)	
309.84	337.56	2.66	4.48	3.07		0.172	
F_{Y1}	F_{Y2}	K_{Y1}	K_{Y2}	K_{Y3}		NL(X)	
1416.87	1416.87	40.13	8.89	21.51		0.115	
F_{X1}	F_{X2}	K_{X1}	K_{X2}	K_{X3}		H_Y	
746.52	746.52	20.72	6.63	12.09		0.096	
		U_Y	U_X			H_X	
		2.53	2.53			0.073	

* F_{Z1} represents the yield bearing capacity (unit: kN) loaded in the Z-axis direction, and F_{Z2} represents the ultimate bearing capacity (unit: kN) loaded in the Z-axis direction; F_{Y1} and F_{Y2} represent the positive and negative maximum horizontal thrust (unit: kN) loaded in the Y-axis direction; F_{X1} and F_{X2} represent the positive and negative maximum horizontal thrust (unit: kN) loaded in the X-axis direction; K_{Z1} represents the initial stiffness of the Z-axis loading member (unit: kN/mm), K_{Z2} represents the yield stiffness of the Z-axis loading member (unit : kN/mm), K_{Z3} represents the ultimate stiffness of the Z-axis loading member (unit: kN/mm); K_{Y1} represents the elastic stiffness of the Y-axis loading member (unit: kN/mm), K_{Y2} represents the plastic stiffness of the Y-axis loading member (unit: kN/mm), and K_{Y3} represents the effective stiffness of the Y-axis loading member (unit: kN/mm). K_{X1} represents the elastic stiffness of the X-axis loading member (unit: kN/mm), K_{X2} represents the plastic stiffness of the X-axis loading member (unit: kN/mm), and K_{X3} represents the effective stiffness of the X-axis loading member (unit: kN/mm). U_Y represents the ductility of the member along the Y axis, U_X represents the ductility of the member along the X axis; NL(Y) and NL(X) represent the nonlinear coefficients of the components along the Y-axis and X-axis directions; H_Y and H_X represent the equivalent viscous damping coefficients of the components along the Y-axis and X-axis directions.

CONCLUSIONS

1. The static structural behavior of the 'Five-tier Outer Eave Column-head Dougong Bracket' test model from Nanchan Temple's Main Hall (Tang Dynasty) under the Z-axis vertical monotonic static load can be described by the variable stiffness linear elastic mechanical model. The static structural behavior under the quasi-static load of low-cycle reciprocating load on the Y-axis and X-axis can be described by the restoring force model.
2. At the strength level, the yield bearing capacity of Tang Dynasty Dougong Bracket test model on the Z-axis is 310 kN, and the ultimate bearing capacity is 338 kN; the maximum horizontal thrust on the Y axis is 1417 kN; the maximum forward horizontal thrust on the X-axis is 747 kN.
3. At the deformation level, the initial stiffness of the Tang Dynasty Dougong Bracket test model on the Z axis is 2.66 kN/mm, the yield stiffness is 4.48 kN/mm, and the deformation stiffness is 3.07 kN/mm. The elastic stiffness on the Y axis is 40.13 kN/mm, the plastic stiffness is 8.89kN / mm, the effective stiffness is 21.51kN / mm, and the ductility is 2.53. The elastic stiffness on the X-axis is 20.72 kN/mm, the plastic stiffness is 6.63 kN/mm, the effective stiffness is 12.09 kN/mm, and the ductility is 2.53.

4. At the energy level, the nonlinear coefficient of the Tang Dynasty Dougong Bracket test model on the Y axis is 0.172, and the equivalent viscous damping coefficient is 0.096. The nonlinear coefficient on the X-axis is 0.115, and the equivalent viscous damping coefficient is 0.073.
5. The finite element methodology successfully validated the Dougong bracket's structural efficacy through comprehensive mechanical indices (ultimate bearing capacity: 338 kN, ductility: 2.53), confirming the Tang Dynasty builders' design as a mechanically optimized solution that harmonized load transfer efficiency with seismic resilience.

ACKNOWLEDGMENTS

This work was supported by the Fundamental Research Funds for Inner Mongolia University of Science & Technology (Grant No. 2024QNJS023) and the Scientific Research Projects of First-class Disciplines (Grant No. YLXKZX-NKD-027).

REFERENCES CITED

Bedon, C., Fragiacomo, M., Amadio, C., and Sadoch, C. (2015). "Experimental study and numerical investigation of Blockhaus shear walls subjected to in-plane seismic loads," *Journal of Structural Engineering* 141(4), article 04014118. DOI: 10.1061/(ASCE)ST.1943-541X.0001065

Chen, Z., Zhu, E., Lam, F., and Pan, J. (2014). "Structural performance of Dou-Gong brackets of Yingxian Wood Pagoda under vertical load-An experimental study," *Engineering Structures* 80, 274-288. DOI: 10.1016/j.engstruct.2014.09.013

Chen, J., Chen, Y. F., Shi, X., Zhao, Y., and Li, T. (2018). "Hysteresis behavior of traditional timber structures by full-scale tests," *Advances in Structural Engineering* 21(2), 287-299. DOI: 10.1177/1369433217717117

Cao, J., Zhao, Y., Liu, Y., Lu, H., and Wang, W. (2021). "Load-carrying capacity analysis of traditional Chinese Dou-gong joints under monotonic vertical and reversal lateral loading," *Journal of Building Engineering* 44, article 102847. DOI: 10.1016/j.jobe.2021.102847

D'Ayala, D. F., and Tsai, P. H. (2008). "Seismic vulnerability of historic Dieh–Dou timber structures in Taiwan," *Engineering Structures* 30, 2101-2113. DOI: 10.1016/j.engstruct.2007.11.007

Fang, D. P., Iwasaki, S., Yu, M. H., Shen, Q. P., Miyamoto, Y., and Hikosaka, H. (2001). "Ancient Chinese timber architecture. II: Dynamic characteristics," *Journal of Structural Engineering* 127(11), 1358-1364. DOI: 10.1061/(ASCE)0733-9445(2001)127:11(1358)

Fujita, K., Kimura, M., Ohashi, Y., and Sakamoto, I. (2001). "Hysteresis model and stiffness evaluation of bracket complexes used in traditional timber structures based on static lateral loading tests," *Journal of Structural and Construction Engineering* 66(543), 121-127. DOI: 10.3130/aijs.66.121_2

GB/T 1933 (2009). "Method for determination of the density of wood," Standardization Administration of China, Beijing, China.

GB/T 15777 (2017). "Method for determination of the modulus of elasticity in compression parallel to grain of wood," Standardization Administration of China, Beijing, China.
GB/T 1943 (2009). "Method for determination of the modulus of elasticity in compression perpendicular to grain of wood," Standardization Administration of China, Beijing, China.
GB/T 1935 (2009). "Method of testing in compressive strength parallel to grain of wood," Standardization Administration of China, Beijing, China.
GB/T 1939 (2009). "Method of testing in compression perpendicular to grain of wood," Standardization Administration of China, Beijing, China.
GB/T 1936.1 (2009). "Method of testing in bending strength of wood," Standardization Administration of China, Beijing, China.
LY/T 3297 (2022). "Dynamic test method for shear modulus of wood," Standardization Administration of China, Beijing, China.
Meng, X., Yang, Q., Wei, J., and Li, T. (2018). "Experimental investigation on the lateral structural performance of a traditional Chinese pre-Ming dynasty timber structure based on half-scale pseudo-static tests," *Engineering Structures* 167, 582-591. DOI: 10.1016/j.engstruct.2018.04.077
Meng, X., Li, T., Yang, Q., and Wei, J. (2018). "Seismic mechanism analysis of a traditional Chinese timber structure based on quasi-static tests," *Structural Control Health Monitoring* 25(10), article e2245. DOI: 10.1002/stc.2245
Meng, X., Li, T., and Yang, Q. (2019). "Experimental study on the seismic mechanism of a full-scale traditional Chinese timber structure," *Engineering Structures* 180, 484-493. DOI: 10.1016/j.engstruct.2018.11.055
Niu, Q. (2017). *Experimental Study and Theoretical Analysis on Half-Scale Model of Timber Structure in Song Dynasty*, Master's Thesis, Taiyuan University of Technology, Taiyuan, China.
Sciomenta, M., Bedon, C., Fragiacomo, M., and Luongo, A. (2018). "Shear performance assessment of timber log-house walls under in-plane lateral loads via numerical and analytical modelling," *Buildings* 8(8), article 99. DOI: 10.3390/buildings8080099
Sha, B., Xie, L., Yong, X., and Li, A. (2021). "An experimental study of the combined hysteretic behavior of dougong and upper frame in Yingxian Wood Pagoda," *Construction and Building Materials* 305, article ID 124723. DOI: 10.1016/j.conbuildmat.2021.124723
Suzuki, Y., and Maeno, M. (2006). "Structural mechanism of traditional wooden frames by dynamic and static tests," *Structural Control Health Monitoring* 13, 508-522. DOI: 10.1002/stc.153
Wu, Y., Song, X., Ventura, C., and Lam, F. (2020). "Modeling hysteretic behavior of lateral load-resisting elements in traditional Chinese timber structures," *Journal of Structural Engineering* 146(5), article 04020062. DOI: 10.1061/(ASCE)ST.1943-541X.0002613
Wu, Y., Song, X., Gu, X., and Luo, L. (2018). "Dynamic performance of a multi-story traditional timber pagoda," *Engineering Structures* 159, 277-285. DOI: 10.1016/j.engstruct.2018.01.003
Xue, J. Y., Wu, Z. J., Zhang, F. L., and Zhao, H. T. (2016). "Seismic damage evaluation model of Chinese ancient timber buildings," *Advances in Structural Engineering* 18(10), 1671-1683. DOI: 10.1260/1369-4332.18.10.1671

Yao, L. and Li, Y. (2023). "Simulation study on static characteristics of Qing-style 'One Bucket Three Liters' column-cap Dou-Gong bracket," *BioResources* 18(4), 6955-6970. DOI: 10.15376/biores.18.4.6955-6970

Article submitted: April 6, 2025; Peer review completed: May 10, 2020; Revised version received: May 13, 2025; Accepted: June 2, 2025; Published: June 11, 2025.
DOI: 10.15376/biores.20.3.6082-6099